APS physics

CHORUS
Clearinghouse for the Open Research of the United States

This is the accepted manuscript made available via CHORUS, the article has been published as:

Quantitative comparison of the isotropic and anisotropic Maxwellian velocity space distribution function models in a dusty plasma

R. Fisher and E. Thomas, Jr.

Phys. Rev. E **86**, 066403 — Published 6 December 2012

DOI: 10.1103/PhysRevE.86.066403

Quantitative comparison of the isotropic and anisotropic Maxwellian velocity space distribution function models in a dusty plasma

R. Fisher and E. Thomas, Jr.

Auburn University

Measurements of the velocity space distribution in a weakly coupled dusty plasma are modeled with both the spherically symmetric Maxwellian probability distribution function and the ellipsoidally symmetric tri-normal probability distribution function. The effectiveness of the two models is compared quantitatively using an application of Bayesian probability theory which shows that the anisotropy included in the tri-normal model provides a much improved description of the system.

I. INTRODUCTION

The study and classification of plasmas is frequently based on a fluid model of the system. With this approach the various components of a plasma are each described by their distribution in phase space. The phase space is a seven dimensional space composed of three configuration space, three velocity space, and one time dimension. In plasma systems that are considered to be in, or near, a state of equilibrium the velocity space distribution is typically modeled with the spherically symmetric Maxwellian distribution function [1].

Laboratory based dusty plasmas provide a convenient system in which the properties of a fluid system can be studied in great detail. A dusty plasma is a system in which a population of charged microparticles (i.e. the "dust" particles) is embedded in a plasma environment of electrons, ions, and neutral gas. A photograph of a cross section of the dusty plasma structure (the "dust cloud") discussed below is shown in Fig. 1. In such systems the dust grains acquire a charge by collecting ambient electrons and ions from the background plasma in low energy collisions. Because the electron mobility is higher than that of the ions in most laboratory studies, a dust grain typically collects an excess of electrons and acquires a net negative charge of several hundred to several thousand electrons depending upon the size of the grain and the plasma parameters [2]. However, compared to the electron and ion components of the plasma, the dust particles are quite massive ($m_d \geq 10^{12} m_{ion}$) resulting in a relatively small charge to mass ratio, which causes the dust component to operate on long time scales compared to the other plasma components. The result is that the dust particles form a component of the plasma that fully participates in the system dynamics, but that is composed of particles that are large and slow enough so that direct optical imaging can be used to make detailed measurements of the dust component properties.

Recent studies of weakly-coupled (fluid-like) dusty plasmas has shown, qualitatively, that the standard Maxwellian model provides an inadequate description of measured dust component velocity space distributions [3–10]. A generalization of the Maxwellian distribution, the tri-normal distribution function (or the Maxwellian distribution with tensor variance), was found to provide a better description of the system. In this paper we report the results of an experiment in which the velocity space distribution of the dust component of a plasma was measured and where the necessity of applying the more general model of the velocity space is shown quantitatively.

II. MODELS OF THE VELOCITY SPACE

The phase space distribution used to describe a component of a plasma as a fluid, $f\left(\vec{r},\vec{v},t\right)$, is the product of the number density, $n\left(\vec{r},t\right)$, and the velocity space distribution function, $F\left(\vec{r},\vec{v},t\right)$. In the experiment described here the dust cloud was observed to be macroscopically mechanically stable and free of apparent wave activity or large-scale dust transport for time periods of hours, which allows the time dimension of phase space to be omitted in what follows. Thus, the phase space distribution for the system is given by:

$$f\left(\vec{r},\vec{v}\right)=n\left(\vec{r}\right)F\left(\vec{r},\vec{v}\right). \tag{1}$$

The standard assumption is that the velocity distribution function in Eq. (1) is the Maxwellian probability distribution function.

The three dimensional Maxwellian probability distribution function, $F_m\left(\vec{v}\right)$, is given by:

$$F_m\left(\vec{v}\right) = \left(2\pi\right)^{-3/2} \sigma_m^{-3} \exp\left[\frac{-\left(\vec{v}-\vec{u}\right)^2}{2\sigma_m^2}\right] \tag{2}$$

Where $\vec{v}$ is the three dimensional velocity vector, $\vec{u}$ is the three dimensional drift velocity vector, and σ_m is the scalar standard deviation of the velocity space. The fact that the standard deviation (and variance) is scalar gives the distribution spherical symmetry in velocity space.

The tri-normal probability distribution function [11] is a generalization of the Maxwellian distribution function that features tensor variance. The tri-normal distribution is given by:

$$F_{tn}\left(\vec{v}\right) = \left(2\pi\right)^{-3/2} \left|\overline{\overline{\Sigma}}\right|^{-1/2} exp\left(\frac{-1}{2}\left(\vec{v}-\vec{u}\right)^{\dagger} \cdot \overline{\overline{\Sigma}}^{-1} \cdot \left(\vec{v}-\vec{u}\right)\right) \tag{3}$$

where $\overline{\overline{\Sigma}}$ is the velocity space covariance tensor. In the Cartesian coordinate system $\overline{\overline{\Sigma}}$ is given by:

$$\overline{\overline{\Sigma}} = \begin{pmatrix} \sigma_x^2 & \rho_{xy}\sigma_x\sigma_y & \rho_{xz}\sigma_x\sigma_z \\ \rho_{xy}\sigma_x\sigma_y & \sigma_y^2 & \rho_{yz}\sigma_y\sigma_z \\ \rho_{xz}\sigma_x\sigma_z & \rho_{yz}\sigma_y\sigma_z & \sigma_z^2 \end{pmatrix}. \tag{4}$$

The σ_i quantities give the standard deviation of the velocity space in the $\hat{v}_i$ direction and the ρ_{ij} terms give the statistical correlation of the velocity space with respect to the $\hat{v}_i$ and $\hat{v}_j$ directions. The standard deviation and correlation factors are allowed to differ from one another, giving the tri-normal distribution ellipsoidal symmetry in a three dimensional velocity space. The more general ellipsoidal symmetry is what allows the tri-normal distribution to accurately describe the anisotropic velocity space distribution observations discussed below.

It is noted that the canonical Maxwellian distribution function is included in the tri-normal probability distribution as the special case where the covariance tensor is diagonal and isotropic (i.e., when $\overline{\overline{\Sigma}}_m = \sigma_m^2 \overline{\overline{I}}$, where $\overline{\overline{I}}$ is the rank two identity tensor). The two velocity space distribution function models will be compared to the observations and it will be shown that the tri-normal distribution function describes the observations much more completely.

III. EXPERIMENTAL METHODOLOGY

The experiment was performed in the Three -dimensional Dusty Plasma eXperiment (3DPX) at Auburn University. A photograph of 3DPX is shown in Fig. 2 (a) and the orientation of the experimental components is shown schematically in Fig. 2 (b). A dc glow discharge plasma was produced in 132 mTorr of neutral argon by drawing a steady current of 5.37 mA to the anode at approximately 220 V. The grounded dust tray and chamber walls act as the cathode. Typical ion and electron component parameters in the device are: $n_i \approx 10^{14}\, m^3$, $kT_e \approx 2-5eV$, and $kT_i \approx 0.025eV$ [12–15].

A large quantity of solid silica microspheres (i.e., the dust particles) was placed on the surface of the dust tray (the flat gray surface below the dust cloud and laser sheet in Fig. 2 (b)). The microparticles had radii of $r_d = 1.5 \pm 0.75\mu m$ and corresponding masses of $m_d = 3.6 \pm 0.13 \times 10^{-14} kg$. When the plasma is formed in the 3DPX chamber, a small fraction of the particles that were placed on the dust tray are levitated from the dust tray and become trapped in the plasma (the dust cloud of interest contains approximately 3×10^4 particles). These particles become charged by the ambient plasma and, for the plasma conditions noted above, the

charge of each grain is estimated with orbit motion limited theory [2] to be approximately 4400 electrons.

This population of microparticles that is suspended in the background plasma is the thermodynamic system of interest in this paper. These particles are in contact with the ions, electrons, and neutral atoms, but remain isolated from those on the tray. For these studies, great care is taken to ensure that the particle cloud is stable (i.e., no waves or macroscopic flows) and that there are no flows of microparticles in or out of the suspended dust cloud.

The velocity space distributions for the dust component were measured with the stereoscopic particle image velocimetry (PIV) diagnostic [16]. The diagnostic records images of the cloud with two cameras oriented at different angles with respect to a planar laser sheet that illuminates a cross section of the dust cloud. For a single PIV measurement each of the cameras records two images of the illuminated cross section, separated in time by Δt. The images, and the known Δt, are then used to reconstruct three dimensional velocity vectors within small regions ("volume elements") of the dust cloud each of which was approximately $5.8\times10^{-9}\ m^3$ in this study (the volume elements were approximately 1.7 mm by 1.7 mm in the x and y directions, in the plane of the laser sheet, and 2 mm in the z direction, the thickness of the laser sheet). The particles in each volume element were measured 1500 times in order to build an independent, measured, velocity distribution of the dust component within each volume element.

The uncertainty in the PIV diagnostic was quantified by performing a so-called zero displacement test [4,17]. The process gave measured three dimensional velocity distributions (and systematic uncertainties) for the 853 independent volume elements that made up the dust cloud structure.

IV. DATA ANALYSIS

A. Overview

The measured velocity space distributions were analyzed with a relatively simple application of Bayesian probability theory [18]. This formulation of probability theory contains convenient methods for the inclusion of finite measurement uncertainty (as measured by the zero-displacement test) and for comparing the effectiveness of various models given the same data set. The model comparison procedure described in this section was applied, independently, to the measured velocity space distribution in each of the 853 volume elements within the dust cloud.

In order to compare the performance of two models given the same data set (referred to as "D") and experimental configuration (or background information, "I"), a quantity known as the posterior probability is calculated for each model (the tri-normal distribution "TN" and the Maxwellian distribution "M"). The posterior probability values that are obtained with each model are then compared by taking the ratio:

$$K \equiv \frac{prob(TN \mid D, I)}{prob(M \mid D, I)} \tag{5}$$

The quantity in the numerator of Eq. (5) is the posterior probability for the tri-normal model, the term is read as "the probability of the tri-normal model given the data set and the information". The quantity in the denominator of Eq. (5) is the posterior probability for the Maxwellian model given the same data set and background information. If the value of K is greater than unity the

tri-normal model is said to be the preferred model, if K is less than one the Maxwellian model is selected. Effects such as the finite, known, measurement error and parameter value uncertainty are included in the expressions for each of the posterior probabilities. The process automatically includes a mechanism that penalizes each model for any parameters that are not found in the alternate model.

This is particularly convenient in this context because the two models of interest are quite similar; if one takes a data set and uses two similar models to describe the observations the model with the most parameters will always provide a better "fit" to the data. This type of analysis allows one to determine, quantitatively, if the extra parameters in the more complex model meaningfully contribute to the description of the system or if they simply fit the data better due to the extra freedom in parameter space. A comparison of the two models of interest here shows that the Maxwellian distribution has one independent parameter (σ_m) and the tri-normal distribution has six independent parameters ($\sigma_x, \sigma_y, \sigma_z, \rho_{xy}, \rho_{yz}$, and ρ_{xz}), the comparison of the efficacy of the two models clearly needs to penalize the tri-normal model for its many extra parameters.

The expression for K, given in Eq. (5), requires simplification before it can be used to compare the models; Bayes' theorem, the Bayesian product rule, and marginalization are applied to give the following expression:

$$K = \frac{prob(D \mid TN, I)}{prob(D \mid M, I)} \frac{prob(TN \mid I)}{prob(M \mid I)}. \tag{6}$$

The left-most ratio on the right hand side of Eq. (6) is the ratio of the likelihood of the data set given each model and information. The right-most ratio in Eq. (6) is the ratio of the prior

probabilities of each model given the available information. Here, the ratio of prior probabilities is chosen to be unity, in order to make a "fair" comparison. With this choice the expression for K reduces to the ratio of the likelihood values for the data set given each of the models:

$$K = \frac{prob(D \mid TN, I)}{prob(D \mid M, I)}. \tag{7}$$

The remainder of the process for finding the K value involves repeated use of the product and marginalization rules for each likelihood function, finding the parameter values, and the associated uncertainties (a detailed discussion of the procedure can be found in [4]).

B. Distribution function parameter estimation

The parameters found within each model are estimated within each volume element. The velocity vectors measured within each volume element are analyzed separately but with the same general process. The drift velocity is calculated in exactly the same way for both models and is discussed in Section IV.B.1, the width and shape characterization of the measurements are discussed in Sections IV.B.2 and IV.B.3 for the Maxwellian and tri-normal models, respectively.

1. The drift velocity

The fluid drift velocity is the average velocity of the particles within a given volume element. This information is given by the three drift velocity vector components:

$$\bar{u} = u_x \hat{x} + u_y \hat{y} + u_z \hat{z}. \tag{8}$$

The data set consists of N velocity vector measurements, the kth measured vector has the form:

$$D_k = v_{k,x} \hat{x} + v_{k,y} \hat{y} + v_{k,z} \hat{z}. \tag{9}$$

The drift vector is given by the mean value of the vector components of the measurements:

$$u_i = \frac{1}{N}\sum_{k=1}^{N} u_{k,i} \tag{10}$$

Where $i = x, y, z$. This process is the same for both models. For simplicity the drift vector results are recorded and the data are shifted to their respective rest frames in the parameter estimation process that is described below.

2. Maxwellian distribution parameters

The Maxwellian distribution function is given by Eq. (2), the remaining parameter that must be found is the standard deviation, σ_m. We begin by obtaining an expression for the likelihood of the data given the Maxwellian model, the denominator of the ratio on the right hand side of Eq. (7), and apply the marginalization and product rules:

$$prob(D \mid M, I) = \int prob(D \mid \sigma_m, M, I)\, prob(\sigma_m \mid M, I)\, d\sigma_m \tag{11}$$

The last term in the integrand is the prior probability of the scalar standard deviation given the Maxwellian model and the available information. The prior probability term encodes our *a priori* knowledge of the values that the parameter σ_m can have. Here, and in all of the following discussion, we assume a uniform prior probability distribution for the parameter, which is non-zero for reasonable values of the parameter. We use a normalized step function for the prior probability of σ_m:

$$prob(\sigma_m \mid M, I) = \begin{cases} \dfrac{1}{\sigma_{\max} - \sigma_{\min}} & \sigma_{\min} < \sigma_m \le \sigma_{\max} \\ 0 & elsewhere \end{cases} \tag{12}$$

The standard deviation must be positive so $\sigma_{\min} = 0$ and a cursory examination of the data revealed that the distribution widths are all less than 0.1 m/sec, which is chosen as the maximum value.

The first term found within the integrand of Eq. (11) is the likelihood of the data given the parameter, the model, and the information. We assume that our parameter estimate will have an optimal value, σ_{m0}, and a normally distributed uncertainty about the optimal value, $\delta\sigma_m$. We include this information in the likelihood function via convolution:

$$prob\left(D \mid \sigma_m, M, I\right) = prob\left(D \mid \sigma_{m0}, M, I\right) \exp\left[\frac{-\left(\sigma_m - \sigma_{m0}\right)^2}{2\left(\delta\sigma_m\right)^2}\right] \tag{13}$$

The final consideration before proceeding to find the actual likelihood value is the inclusion of finite measurement uncertainty. We model the data from the zero-displacement test (data set "Z") with a tri-normal distribution with covariance tensor $\overline{\overline{\varepsilon}}$. The elements of $\overline{\overline{\varepsilon}}$ are found by taking the sample covariance of the zero-displacement test data:

$$\varepsilon_{ij} = \frac{1}{N-1}\sum_{k=1}^{N_z}\left(Z_{ki} - \left\langle Z_i \right\rangle\right)\left(Z_{kj} - \left\langle Z_j \right\rangle\right)\hat{e}_i\hat{e}_j \tag{14}$$

Where the angle brackets indicate the mean of the vector component in the data set. This information is incorporated in the likelihood function with the product and marginalization rules. The result, after integration and algebra, is the likelihood function for the data given the parameter, the Maxwellian model, and the associated information:

$$prob\left(D \mid \sigma_m, M, I\right) = \exp\left[\frac{-\left(\sigma_m - \sigma_{m0}\right)}{2\delta\sigma_m^2}\right]\left(2\pi\right)^{-3N/2}\left|\overline{\overline{\varepsilon}} + \sigma_{m0}^2\overline{\overline{I}}\right|^{-N/2}\exp\left[\frac{-1}{2}\sum_{k=1}^{N}\vec{v}_k^{\dagger}\cdot\left(\overline{\overline{\varepsilon}} + \sigma_{m0}^2\overline{\overline{I}}\right)^{-1}\cdot\vec{v}_k\right] \tag{15}$$

where the vertical bars indicate a determinant and $\vec{v}_k^{\dagger}$ indicates the transpose of the kth data vector.

The optimal standard deviation value, σ_{m0}, is found by maximizing the likelihood function given in Eq. (15). This is accomplished by minimizing the first partial derivative of the likelihood function's natural logarithm:

$$0 = \left. \frac{\partial \ln prob\left(D \mid \sigma_m, M, I\right)}{\partial \sigma_{m0}} \right|_{\sigma_m = \sigma_{m0}} \tag{16}$$

The uncertainty in the optimal parameter value, $\delta\sigma_m$, is found by minimizing the second derivative of the likelihood function's natural logarithm:

$$0 = \left. \frac{\partial^2 \ln prob\left(D \mid \sigma_m, M, I\right)}{\partial \sigma_{m0}^2} \right|_{\sigma_m = \sigma_{m0}} \tag{17}$$

With the parameter value estimate process completed, Eqs. (12) and (15) can be inserted into Eq. (11) to give the likelihood of the data set given the Maxwellian model:

$$\begin{aligned} prob\left(D \mid M, I\right) &= \left(2\pi\right)^{-3N/2} \left| \bar{\bar{\varepsilon}} + \sigma_{m0}^2 \bar{\bar{I}} \right|^{-N/2} \sqrt{\frac{\pi}{2}} \frac{\delta\sigma_m}{\sigma_{\max}} \times \\ &\left[erf\left(\frac{\sigma_{m0}}{\sqrt{2}\delta\sigma_m} \right) - erf\left(\frac{\sigma_{m0} - \sigma_{\max}}{\sqrt{2}\delta\sigma_m} \right) \right] \exp\left[\frac{-1}{2} \sum_{k=1}^{N} \vec{v}_k^{\dagger} \cdot \left(\bar{\bar{\varepsilon}} + \sigma_{m0}^2 \bar{\bar{I}} \right)^{-1} \cdot \vec{v}_k \right] \end{aligned} \tag{18}$$

Which is the quantity that appears in the denominator of the expression for the ratio of posterior probabilities, Eq. (7).

3. Tri-normal distribution parameters

The process for finding the optimal parameter values, uncertainties, and the likelihood function for the data given the tri-normal model and the available information follows the same process as was used for the Maxwellian model. The difference is that there are now six unknown parameter values, which significantly increases the amount of algebra. The results for the important quantities are given below; the algebra is omitted for brevity. In all cases the prior probability distributions for the parameters are assumed uniform; for the standard deviation parameters the range of allowed values is the same as for the Maxwellian model, for the correlation parameters we allow the parameter value to fall anywhere in the allowed range, $-1 < \rho_{ij} < 1$.

The likelihood function for the data given the parameters, the tri-normal model, and the available information (analogous to Eq. (15)) is given by:

$$prob\left(D \mid \overline{\overline{\Sigma}}, TN, I\right) = (2\pi)^{-3N/2} \left|\overline{\overline{\varepsilon}} + \overline{\overline{\Sigma}}_0\right|^{-N/2} \exp\left[\frac{-(\sigma_x - \sigma_{x0})^2}{2\delta\sigma_x^2} - \frac{(\sigma_y - \sigma_{y0})^2}{2\delta\sigma_y^2} - \frac{(\sigma_z - \sigma_{z0})^2}{2\delta\sigma_z^2}\right] \times$$
$$\exp\left[-\frac{(\rho_{xy} - \rho_{xy0})^2}{2\delta\rho_{xy}^2} - \frac{(\rho_{yz} - \rho_{yz0})^2}{2\delta\rho_{yz}^2} - \frac{(\rho_{xz} - \rho_{xz0})^2}{2\delta\rho_{xz}^2}\right] \exp\left[\frac{-1}{2}\sum_{k=1}^{N} \vec{v}_k^{\dagger} \cdot \left(\overline{\overline{\varepsilon}} + \overline{\overline{\Sigma}}_0\right)^{-1} \cdot \vec{v}_k\right] \quad (19)$$

Where $\overline{\overline{\Sigma}}_0$ is the optimal covariance tensor:

$$\overline{\overline{\Sigma}}_0 = \begin{bmatrix} \sigma_{x0}^2 & \rho_{xy0}\sigma_{x0}\sigma_{y0} & \rho_{xz0}\sigma_{x0}\sigma_{z0} \\ \rho_{xy0}\sigma_{x0}\sigma_{y0} & \sigma_{y0}^2 & \rho_{yz0}\sigma_{y0}\sigma_{z0} \\ \rho_{xz0}\sigma_{x0}\sigma_{z0} & \rho_{yz0}\sigma_{y0}\sigma_{z0} & \sigma_{z0}^2 \end{bmatrix} \quad (20)$$

The optimal parameter values and the uncertainties are found by minimizing the partial derivatives of the natural logarithm of Eq. (19) with respect to each parameter and solving the resulting system of coupled equations.

The final quantity that is required for the model comparison is the likelihood function of the data given the tri-normal distribution and the information. It can be shown that the likelihood function is given by:

$$
\begin{aligned}
&prob\left(D \mid TN, I\right) = \left(\frac{10\pi}{4}\right)^{3} \delta\sigma_x \delta\sigma_y \delta\sigma_z \delta\rho_{xy} \delta\rho_{yz} \delta\rho_{xz} \times \\
&\left[erf\left(\frac{\sigma_{x0}}{\sqrt{2}\delta\sigma_x}\right) - erf\left(\frac{\sigma_{x0}-\sigma_{\min}}{\sqrt{2}\delta\sigma_x}\right)\right]\left[erf\left(\frac{\sigma_{y0}}{\sqrt{2}\delta\sigma_y}\right) - erf\left(\frac{\sigma_{y0}-\sigma_{\min}}{\sqrt{2}\delta\sigma_y}\right)\right] \times \\
&\left[erf\left(\frac{\sigma_{z0}}{\sqrt{2}\delta\sigma_z}\right) - erf\left(\frac{\sigma_{z0}-\sigma_{\min}}{\sqrt{2}\delta\sigma_z}\right)\right]\left[erf\left(\frac{1-\rho_{xy0}}{\sqrt{2}\delta\rho_{xy}}\right) + erf\left(\frac{1+\rho_{xy0}}{\sqrt{2}\delta\rho_{xy}}\right)\right] \times \\
&\left[erf\left(\frac{1-\rho_{yz0}}{\sqrt{2}\delta\rho_{yz}}\right) + erf\left(\frac{1+\rho_{yz0}}{\sqrt{2}\delta\rho_{yz}}\right)\right]\left[erf\left(\frac{1-\rho_{xz0}}{\sqrt{2}\delta\rho_{xz}}\right) + erf\left(\frac{1+\rho_{xz0}}{\sqrt{2}\delta\rho_{xz}}\right)\right] \times \\
&\left(2\pi\right)^{-3N/2} \left|\overline{\overline{\varepsilon}} + \overline{\overline{\Sigma}}_0\right|^{-N/2} \exp\left[\frac{-1}{2}\sum_{k=1}^{N} \vec{v}_k^{\dagger} \cdot \left(\overline{\overline{\varepsilon}} + \overline{\overline{\Sigma}}_0\right)^{-1} \cdot \vec{v}_k\right]
\end{aligned}
\tag{21}
$$

These expressions allow us to proceed to the quantitative comparison of the performance of the velocity space models.

V. RESULTS

A. Single volume element

In this section the result of the analysis process described in Section IV is shown for a single volume element within the dust cloud. An example of the measured distribution, in a two dimensional sub-space, is shown in Fig. 3. In two dimensions the standard Maxwellian distribution function is circularly symmetric. The histogram shown in Fig. 3 clearly exhibits the elliptical symmetry that is the signature of the two-dimensional version of the tri-normal

distribution function model. The drift velocity vector, optimal parameter values, and parameter value uncertainties were calculated for these data as described above; the results were then used to find the ratio of posterior probabilities for the two models given the same data set by inserting Eqs. (18) and (21) into Eq. (7). For the volume element shown in Fig. 3 the result was $K = 1.03 \times 10^{164}$, which is much larger than unity, indicating that the tri-normal model does a much better job of describing the data than the standard Maxwellian model. Similar results will be shown to be systematic throughout all the volume elements within the dust cloud structure but first the very large magnitude of K will be addressed.

B. Large data set effects

The extremely large posterior probability ratio found in the previous section is the result of the data set size that was used in the analysis process. To show the effect of the large amount of data used in this study smaller subsets of the measured vectors from the volume element were analyzed. Fig. 4 shows the base ten logarithm of the posterior probability ratio as a function of the number of vectors in the subset. Subsets containing 10, 20, 30, 50, 75, 100, 200, 300, 500, 750, and 1000 vectors were randomly selected from the full data set and the K ratio value was computed. This was repeated for 400 different random samples at each subset size. The black points in Fig. 4 indicate the average K value from the 400 subsets and the red bars show the standard deviation of the K value from the 400 subsets. It can be seen that the extremely high K value for the full set of measurements, from which the sub-sets discussed above were selected, is simply the result of the data set size.

Fig. 4 (b) shows the results of the subset sampling for low data set size; if less than approximately 50 measurements are considered then uncertainties associated with small sample

size swamp the posterior probability ratio calculation. In the regime of small sample size the performance of the two models is, for practical purposes, statistically indistinguishable. The typical data set size used in previous studies reporting anisotropic velocity space distributions for weakly coupled dusty plasmas [7–9,17,19] fell into the range shown in Fig. 4 (b). By increasing the number of sampled velocity vectors we were able to decrease the statistical uncertainty in the parameter values which allows easy discrimination between the two models. The application of the tri-normal model removes the ambiguity associated with the anisotropy and is a compact extension of the earlier work.

C. All volume elements

The posterior probability ratio for all of the volume elements within the dust cloud is shown as a histogram in Fig. 5. The histogram shows the base ten logarithm of K for the volume elements within the interior of the cloud. The volume elements located on the cloud boundary are omitted because the number of velocity vectors reconstructed with the PIV system was generally lower than in the volume elements found within the interior of the cloud. The histogram shows that in all of the volume elements the posterior probability ratio gave values that strongly favor the tri-normal model of the velocity space.

VI. DISCUSSION AND CONCLUSIONS

A relatively simple application of Bayesian probability theory was presented which allowed the standard Maxwellian and the more general tri-normal models of the velocity space to be compared quantitatively. The results showed that the tri-normal distribution function was the preferred model for describing the velocity space measurements in all of the volume elements

within the dust cloud. The observed anisotropy in velocity space is consistent with what has been seen qualitatively in previous studies; it is shown here that the anisotropy is systematically and quantitatively important throughout the entire system. By accounting for finite measurement error and extra model parameter effects it was shown that the anisotropy is not a relic of the measurement process or a small, perturbation level, effect.

The tri-normal probability distribution function is the simplest multi-dimensional generalization of the Maxwellian probability distribution function that is available and, interestingly, was the original probability distribution function obtained by Clerk-Maxwell before simplifying assumptions were made to give the ubiquitous Maxwellian distribution. The more general model accounts for the anisotropy that is commonly observed in plasma-fluid measurements in a convenient extension of the standard picture.

Acknowledgements:

This work is supported by grants from the National Science Foundation (PHY- 0810419) and NASA (NNX10AR53G).

References:

[1] J. Clerk-Maxwell, Philosophical Transactions of the Royal Society of London. **157**, 49–88 (1867).

[2] P. K. Shukla and A. A. Mamun, *Introduction to Dusty Plasmas* (IOP Publishing, LTD, Bristol, 2002).

[3] R. Fisher and E. Thomas, Physics of Plasmas **18**, 113701 (2011).

[4] R. Fisher, Measurement of the Phase Space Distribution in a Complex Plasma, Auburn University, 2012.

[5] B. Liu, J. Goree, and Y. Feng, Physical Review E **78**, 1–10 (2008).

[6] B. Liu and J. Goree, Physical Review Letters **100**, 1–4 (2008).

[7] J. D. Williams and E. Thomas, Physics of Plasmas **14**, 063702 (2007).

[8] J. D. Williams and E. Thomas, Physics of Plasmas **13**, 063509 (2006).

[9] E. Thomas and J. D. Williams, Physics of Plasmas **13**, 055702 (2006).

[10] H. M. Thomas, G. E. Morfill, V. Demmel, J. Goree, B. Feuerbacher, and D. Möhlmann, Physical Review Letters **73**, 652–655 (1994).

[11] L. D. Landau and E. M. Lifshitz, *Course of Theoretical Physics Volume 5. Statistical Physics Part 1*, 3rd ed. (Elsevier Ltd., 1980).

[12] E. Thomas and R. L. Merlino, IEEE Transactions on Plasma Science **29**, 152–157 (2001).

[13] E. Thomas, R. Fisher, and R. L. Merlino, Physics of Plasmas **14**, 123701 (2007).

[14] E. Thomas, Physics of Plasmas **6**, 2672 (1999).

[15] E. Thomas, Physics of Plasmas **13**, 042107 (2006).

[16] E. Thomas, J. D. Williams, and J. Silver, Physics of Plasmas **11**, L37 (2004).

[17] J. D. Williams, Ph.D. Dissertation, Measurement of the Thermal Properties of a Weakly-Coupled Complex (Dusty) Plasma, Auburn University, 2006.

[18] D. S. Sivia and J. Skilling, *Data Analysis: A Bayesian Tutorial*, Second Ed. (Oxford University Press, USA, New York, 2006).

[19] R. Fisher and E. Thomas, IEEE Transactions on Plasma Science **38**, 833–837 (2010).

Figures captions:

Fig.1 (color online): An image of a single cross section of the dust cloud examined in this study. The dust grains (white) are illuminated by a 2 mm thick planar laser sheet and imaged with the stereo-PIV cameras (described in section III). The yellow boxes indicate the extent of the volume elements in the x-y plane (1.7 mm x 1.7 mm).

Fig. 2 (color online): The 3DPX device. (a) A photograph showing the experimental setup used in the experiment. (b) A schematic of the experimental configuration. The anode is electrically biased relative to the dust tray (the lower flat surface) and the vacuum chamber walls (not shown) to generate the plasma. The dust cloud (the black structure above the tray) is illuminated by the PIV laser sheet and imaged with the cameras.

Fig. 3 (color online): Velocity space histogram in the $\{v_x, v_y\}$ sub-space. Example of the velocity vector measurements in a single volume element. The histogram shows the number of velocity vectors with vx and vy components in the indicated range. The distribution shows anisotropy that is not accounted for with the Maxwellian model of the velocity space.

Fig. 4 (color online): Number of measurements vs. K. Plot showing the effect of the large data sets used in the study. The posterior probability ratio was calculated for the data collected in the volume element shown in Fig. 3 using smaller sub-sets of the full data set. The points show the average value of 400 random samples of the full data set for the indicated sub-set size. The red bars indicate the standard deviation of the calculated K ratios. (a) Sub-sets containing 10-1000 vectors. (b) Sub-sets containing 10-100 vectors. The black line indicates a K value of 1, where the models perform identically.

Fig. 5: Histogram showing the base ten logarithm of the posterior probability ratio for all volume elements within the dust cloud. The K values are all much larger than unity which indicates that the tri-normal model describes the system much more completely than the Maxwellian model.

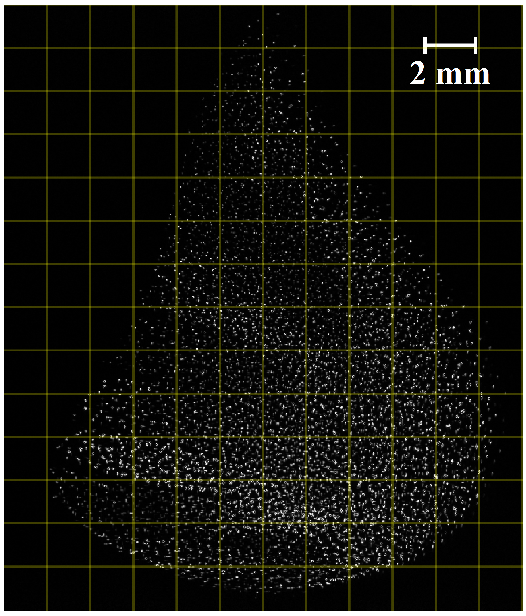

Figure 01 EV10853 19NOV2012

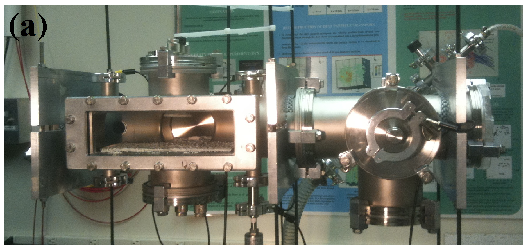

Figure 02a EV10853 19NOV2012

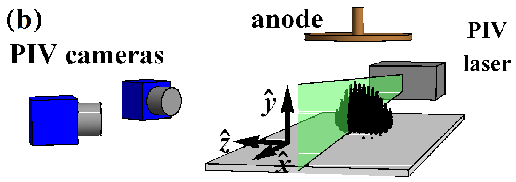

Figure 02b EV10853 19NOV2012

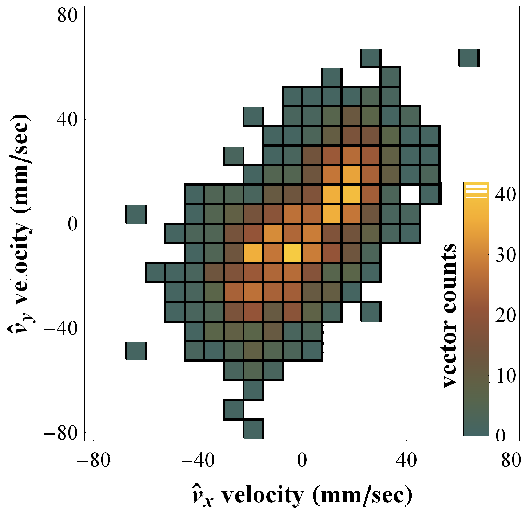

Figure 03 EV10853 19NOV2012

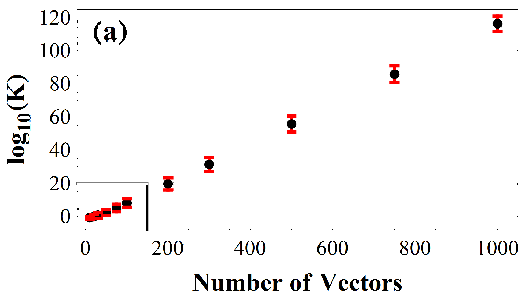

Figure 4a EV10853 19NOV2012

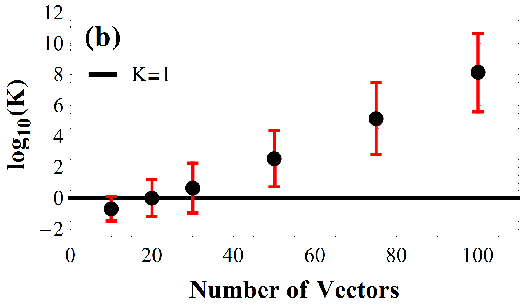

Figure 4b EV10853 19NOV2012

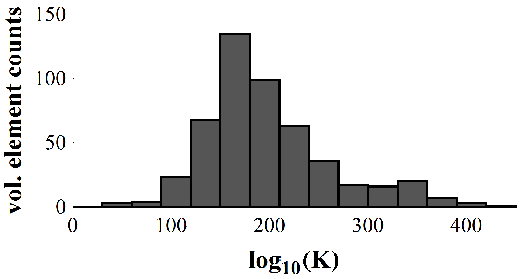

Figure 05 EV10853 19NOV2012